

# Localization from Infinitesimal Kinetic Grading: Critical Scaling and Kibble–Zurek Universality

Argha Debnath, Ayan Sahoo, and Debraj Rakshit

*Harish-Chandra Research Institute, A CI of Homi Bhabha National Institute, Chhatnag Road, Jhunsi, Prayagraj 211 019, India*

We study a one-dimensional lattice model with site-dependent nearest-neighbor hopping amplitudes that follow a power-law profile. The hopping variation is controlled by a grading exponent,  $\alpha$ , which serves as the tuning parameter of the system. In the thermodynamic limit, the ground state becomes localized in the limit  $|\alpha| \rightarrow 0$ , signaling the presence of a critical point characterized by a diverging localization length. Using exact diagonalization methods, we perform finite-size scaling analysis, and extract the associated critical exponent governing the divergence, revealing a universality class distinct from well-known Anderson, Aubry–André and Stark localization. To further characterize the criticality, we analyze inverse participation ratio (IPR), energy gap between the ground and first excited state, and fidelity-susceptibility. We also investigate the nonequilibrium dynamics by linearly ramping the hopping profile at various rates and tracking the evolution of the localization length and the IPR. The Kibble–Zurek mechanism successfully explains the resulting dynamics of the system via the critical exponents obtained from static scaling analysis. Our results demonstrate a clean, disorder-free route to localization and provide a tunable platform relevant to photonic lattices and ultracold atom arrays with engineered hopping profiles.

## I. INTRODUCTION

The localization induced by disorder, proposed by Anderson, is a longstanding research topic in condensed-matter physics [1]. Sufficiently strong disorder suppresses quantum transport, preventing its omnipresence throughout the lattice. Since then, numerous models have explored different ways of introducing randomness to drive the transition between extended and localized phases. Beyond truly random potentials, the Aubry–André model demonstrated that a quasiperiodic modulation can also induce localization through self-duality [2–4]. A third prominent route is Stark localization: a uniform field applied across the lattice suppresses tunneling and leads to spatially localized single-particle states even in the absence of disorder [5–15]. Apart from that, many-body localization in the presence of interaction has attracted a lot of interest in research [16–21]. These theoretical advances have inspired diverse experimental realizations in ultracold atoms, photonic lattices, and solid-state platforms [22–27].

Non-uniform or graded hopping models have been explored in various contexts, including optical lattices and photonic waveguide arrays, where inhomogeneous couplings can induce spatially confined modes [28–35]. However, a systematic analysis of how an infinitesimal gradation in hopping can trigger localization, and how the associated localization transition is characterized in terms of critical exponents and dynamical universality, is still lacking. This motivates a natural set of questions: How does localization emerge under a generic power-law hopping profile? Does a delocalization–localization crossover appear in finite-size systems as  $\alpha$  varies, where  $\alpha$  serves as a control parameter that governs the degree of gradation? More intriguingly, can an infinitesimally small nonlinearity or grading, i.e.  $|\alpha| \rightarrow 0$ , already localize the ground state in the thermodynamic limit? If so, what is the universality class of such a transition, and is it distinct from the well-known Anderson, Aubry–André, or Stark classes?

For  $\alpha = 1$ , the hopping amplitudes grow linearly along the chain, leading to strongly localized eigenstates reminiscent of Stark localization but generated via a graded kinetic term rather than a diagonal potential. Here we treat this case

not as an isolated, previously-known limit, but as a particular representative of a broader class of graded hopping models parametrized by  $\alpha$ , and we focus on how localization emerges as  $|\alpha| \rightarrow 0$ . A key structural feature of the model is that for any nonzero grading exponent  $\alpha > 0$ , the hopping strengths grow boundlessly with the site index, and the local kinetic energy scale therefore becomes non-extensive in the thermodynamic limit, while it vanishes for  $\alpha < 0$ . This makes the limit  $\alpha \rightarrow 0$  intrinsically singular: while  $\alpha = 0$  corresponds to a uniform, translationally invariant and fully delocalized lattice, an arbitrarily small  $\alpha$  produces qualitatively different kinds of kinetic landscapes capable of supporting localization. This sharp distinction motivates a careful study of how localization onsets as  $\alpha$  departs from zero. An intriguing question in this context is if the same scaling exponents may describe the criticality when approached from the either side determined by the sign of  $\alpha$ .

We undertake a detailed characterization of how localization emerges under a power-law grading of the hopping amplitudes. By examining the ground-state wave function, inverse participation ratio, spatial decay profiles, and fidelity susceptibility, we identify a smooth crossover for finite systems but a sharp critical point in the thermodynamic limit. A distinctive feature of the model is that the delocalized regime collapses to the single point  $\alpha = 0$ : the uniform lattice is extended, whereas any infinitesimal grading  $|\alpha| > 0$  eventually produces localized ground states. The transition therefore consists of a sharp critical point at the boundary between a measure-zero delocalized point and a one-sided localized phase. This critical point is characterized by a diverging localization length, a vanishing energy gap, and consistent finite-size scaling of multiple observables, enabling the extraction of critical exponents. Altogether, these results establish a nonlinear, disorder-free universality class that is distinct from those associated with Anderson, Aubry–André, or Stark localization.

The static analysis presented above is complemented by a dynamical study. A central objective of this work is to examine non-equilibrium processes initiated from the ground state deep within the localized phase and subsequently driven

across the transition point. The system experiences a critical slowing down, which leads to an impulse regime near the critical point and the system can no longer adiabatically follow the instantaneous ground state. The quantum Kibble–Zurek mechanism [36–41] in its quantum extension describes how systems deviate from adiabatic evolution, which provides a universal framework for describing defect formation, scaling laws, and non-adiabatic dynamics in the vicinity of continuous phase transitions. The KZM framework has been proven effective in quantum phase transition studies through its application to systems that cross a single quantum critical point under linear or nonlinear ramps [42–49]. Within this approach, the non-equilibrium dynamics near criticality follow universal Kibble–Zurek scaling (KZS), which provides an independent dynamical verification of the critical exponents extracted from the static analysis. Recently, increasing attention has turned toward extending this paradigm to the localization transitions [50–59]. Such studies are gaining importance not only for the advancement of theoretical understanding, but also due to their experimental relevance and potential applications in emerging quantum technologies [60–63].

The organization of the paper is as follows: In Sec. II, we describe our Hamiltonian comprising only with modulated hopping. In Sec. III, we set the background of localization length, inverse participation ratio, fidelity susceptibility. we study the localization properties with modulated hopping coefficient. We perform finite size scaling analysis and extract critical exponents that reveal exotic critical properties of the localization transition. In Sec. IV, we investigate quantum criticality through dynamical driving to study the KZS. In Sec. V, we summarize our results.

## II. MODEL

We consider a one-dimensional tight-binding lattice with site-dependent nearest-neighbor hopping amplitudes following a power-law profile. The Hamiltonian of the system is

$$\hat{H} = - \sum_i i^\alpha \left( \hat{c}_i^\dagger \hat{c}_{i+1} + \hat{c}_{i+1}^\dagger \hat{c}_i \right), \quad (1)$$

where the hopping amplitudes increase (or decrease) monotonically along the chain according to the site index  $i$ . The exponent  $\alpha$  serves as a control parameter that governs the degree of gradation, thereby introducing a spatially varying nonlinearity in the hopping term. Here,  $\hat{c}_i^\dagger$  ( $\hat{c}_i$ ) is the fermionic creation (annihilation) operator at the  $i^{\text{th}}$  site. We impose open boundary condition and investigate finite-size systems by employing the exact diagonalization technique.

The point  $\alpha = 0$  corresponds to the uniform lattice with translational symmetry, where all single-particle states are completely delocalized. However, any nonzero  $\alpha$ , no matter how small, breaks translational invariance and effectively introduces a spatial bias in the hopping landscape. The Hamiltonian contains no on-site terms and consists solely of nearest-neighbor hopping between alternating lattice sites. As a result, it admits a sublattice operator  $\hat{S} = \sum_i (-1)^i |i\rangle\langle i|$  that anti-

commutes with the Hamiltonian,  $\{\hat{S}, \hat{H}\} = 0$ . This immediately implies a spectral mirror symmetry: every eigenstate  $|\psi\rangle$  of energy  $E$  has a partner  $\hat{S}|\psi\rangle$  with energy  $-E$ . Consequently, all nonzero eigenvalues appear in  $\pm E$  pairs, and for lattices of odd size a single zero-energy mode must exist. This structural property is intrinsic to off-diagonal tight-binding models and holds for all values of the grading exponent  $\alpha$ .

The graded tight-binding Hamiltonian introduced above provides a clean, disorder-free setting in which localization emerges solely from a controlled variation of the hopping amplitudes. In the following sections, we analyze this behavior by examining the ground-state localization properties, finite-size scaling, and associated critical exponents, and we subsequently explore the real-time critical dynamics within the Kibble–Zurek framework.

## III. LOCALIZATION TRANSITION AND QUANTUM CRITICALITY

The system is fully delocalized at  $\alpha = 0$ . In order to understand the effect of the graded hopping amplitude, it's important to study the effect of system size. To understand how the graded hopping profile affects this behavior, it is essential to examine its dependence on system size. In order to distinguish the different quantum phases and characterize the criticality, we analyze several key diagnostic quantities, such as localization length, inverse participation ratio, energy gap and fidelity susceptibility. In the following, we study the ground-state behavior of these quantities as the grading exponent  $\alpha$  is varied for different system sizes.

### A. Localization Length

A second-order quantum phase transition is characterized by a diverging length scale of the correlation function. Although the localization transition considered here does not belong to the Landau paradigm, an analogous scaling framework can be formulated in which the localization length plays a role similar to that of the correlation length.

In the present model, the spatial variation of the hopping amplitudes naturally leads to ground states whose support may concentrate near a site. This confinement is naturally quantified by the localization length, which measures how quickly the wave function decays away from its peak. A finite localization length implies that the state is truly localized and largely insensitive to the system size, whereas a diverging localization length signals the approach to a delocalized or critical regime. Thus, tracking how the localization length varies with the grading exponent  $\alpha$  and with system size offers a direct means of identifying the localization-delocalization crossover in the finite-size systems.

The localization length,  $\xi$ , is defined as

$$\xi = \sqrt{\sum_i^L (i - i_c)^2 p_i}, \quad (2)$$

where  $i$  denotes the lattice site,  $p_i$  is the single-particle probability density at site  $i$ , and  $i_c$  is the localisation centre having the expression  $i_c = \sum_i^L i p_i$ . Expanding the  $n^{\text{th}}$  normalized eigenstate of the system,  $|\psi_n\rangle$ , in terms of the single-particle computational basis,  $|i\rangle$ , such that  $|\psi_n\rangle = \sum_i c_n^{(i)} |i\rangle$ ,  $p_i$  is given by  $p_i = |\langle i | \psi_n \rangle|^2 = |c_n^{(i)}|^2$ . For a given control parameter  $g$ , the near-critical scaling of the localization length in the thermodynamic limit is given by

$$\xi \propto |g - g_c|^{-\nu}, \quad (3)$$

where  $g_c$  is the critical point and  $\nu$  is the associated scaling exponent controlling the divergence.

We study the ground state and analyze the dependence of  $\xi$  on the control parameter  $\alpha$  for different system sizes  $L$ . To capture the effect of system size on delocalization-localization transition we have plotted  $\xi$  against  $\alpha$  for various values of  $L$  in Fig. 1(a1) for ground state. This figure illustrates that for finite-sized systems, an initial flat region exists wherein the corresponding wave function exhibits an extended nature. Beyond a certain threshold of  $\alpha$ , say  $\alpha_T$ , the localization length exhibits weak dependence on the system size, leading to the localization of the wave function. The above analysis suggests that the apparent threshold  $\alpha_T(L)$  extracted from finite-size data drifts rapidly toward zero as  $L$  increases. Extrapolating this trend indicates that the limiting value  $\alpha_c \equiv \lim_{L \rightarrow \infty} \alpha_T(L)$  lies extremely close to zero, with numerical estimates yielding a small finite value of order  $10^{-9}$ , which is essentially set by the numerical resolution and the finite system sizes considered in this work.

We perform data collapse for determining the scaling exponent  $\nu$  via the cost function approach (see subsection III E). It offers an unbiased and robust method for extracting the scaling exponents, independent of fitting ambiguities. At the same time, it is an effective approach for overcoming finite-size artefacts. In order to obtain data collapse, we use the following scaling ansatz:

$$\xi/L = f_1 \left( (\alpha - \alpha_c) L^{1/\nu} \right), \quad (4)$$

where  $f_1[\cdot]$  is an arbitrary function. Fig. (a2) displays the data collapse, where we have rescaled the quantities  $\xi$  by  $\xi/L$  and  $\alpha$  as  $(\alpha - \alpha_c) L^{1/\nu}$ . The best data collapse is obtained for  $\nu = 0.49(1)$ . Noticeably, despite qualitatively different kinds of kinetic landscapes on either side of  $\alpha = 0$ , the divergence of the localization length at criticality is governed by the same scaling exponent, which is essentially insensitive to the sign of  $\alpha$ .

It is instructive to contrast the ground-state critical behavior of our model with the well-established one-dimensional localization universality classes. In the Anderson model with weak diagonal disorder, the ground-state localization length

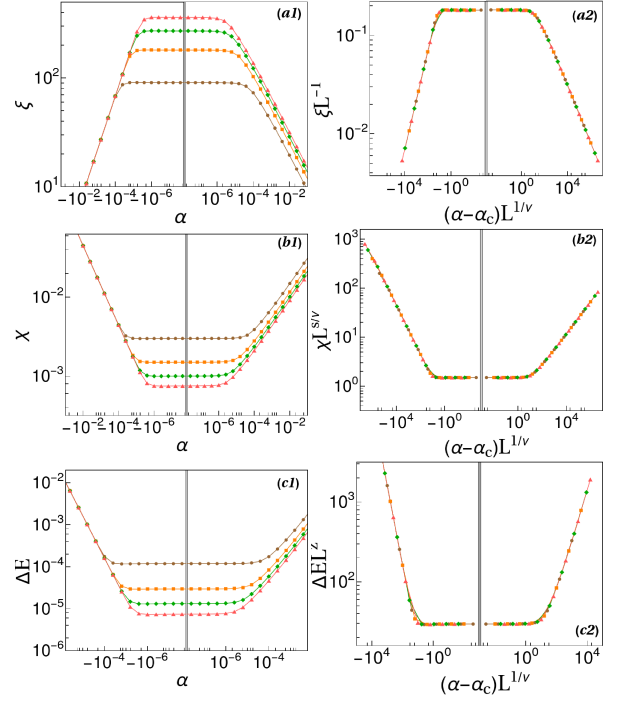


FIG. 1. Variation of (a1) localization length( $\xi$ ), (b1) IPR( $\chi$ ), and (c1) energy gap( $\Delta E$ ) with  $\alpha$  for different system sizes,  $L = 500$  (yellow circle), 1000 (orange square), 1500 (green diamond), 2000 (pink up-triangle) for groundstate using exact diagonalization. Collapse plot with  $(\nu, s, z) \sim (0.49(1), 0.49(1), 2.02(2))$  are shown for (a2)  $\xi$ , (b2)  $\chi$ , (c2)  $\Delta E$  with their re-scaled axis.  $\alpha_c \sim 10^{-9}$

diverges near the band edge with a characteristic exponent  $\nu = 2/3$ . In the Aubry–André–Harper model, the self-duality of the potential ensures an energy-independent transition at a finite potential strength, for which all eigenstates, including the ground state, share the same critical exponent  $\nu = 1$ . In the pure Stark (Wannier–Stark) problem, the band-edge scaling is governed by the Airy equation, giving rise to a much smaller exponent  $\nu = 1/3$ . By contrast, the graded-hopping model studied here exhibits a ground-state localization-length exponent  $\nu \simeq 1/2$ , placing it in a universality class distinct from Anderson, Aubry–André, and Stark localization.

## B. Inverse Participation Ratio

IPR,  $\chi$ , is the next observable that we use for probing the delocalization-localization transition. While the localization length characterizes how rapidly a wavefunction decays away from its localization center, the IPR quantifies the distribution of the weight of the wavefunction across the lattice. It is defined as

$$\chi = \sum_i^L p_i^2. \quad (5)$$

For the delocalized state,  $\chi$  scales as  $\chi \propto L^{-1}$  as the wave function is homogeneously distributed in the lattice. For the

localized state,  $\chi$  has a weak dependence on the system-size. Near criticality, the IPR scales as  $\chi \propto |g - g_c|^s$  in the thermodynamic limit, where  $s$  is another scaling exponent. On the other hand, near criticality, the IPR scales with system size  $L$  as  $\chi \propto L^{-s/\nu}$ .

The variation in the value of the ground state IPR with the increase of  $\alpha$  for different system sizes  $L$  is depicted in Fig. 1(b1). In this figure, up to a certain region of  $\alpha$ , the IPR values are nearly flat, indicating the delocalized nature of the wave function. Beyond this region, the IPR becomes independent of the system size and hence suggests the system's entrance into the localized phase. We consider the following ansatz for extracting the corresponding scaling exponent:

$$\chi = L^{-s/\nu} f_2 \left( (\alpha - \alpha_c) L^{1/\nu} \right), \quad (6)$$

where  $f_2[\cdot]$  is an arbitrary function. By rescaling  $\chi$  and  $\alpha$  as  $\chi L^{s/\nu}$  and  $(\alpha - \alpha_c) L^{1/\nu}$ , respectively, according to Eq. 6, we find that for  $s = 0.49(1)$ , for which we obtain the best data collapse via the cost function approach in Fig. 1(b2).

### C. Energy Gap

As in usual quantum criticality, the energy gap between the first excited state and the ground state can also be used to characterize the criticality. According to the finite-size scaling, the energy gap  $\Delta E$  should scale as  $\Delta E \propto L^{-z}$  at criticality, and when  $L \rightarrow \infty$ ,  $\Delta E$  scales with  $g$  as  $\Delta E \propto g^{-\nu z}$ .

Fig. 1(c1) shows the energy gap  $\Delta E$  with hopping strength  $\alpha$  for different system sizes. A very narrow energy gap in the delocalized phase becomes wider in the localized phase. While in the delocalized regime, the system has a super-extensive dependence on the system size; the dependence drastically in the localized regime, and  $\Delta E$  becomes nearly independent in the localized phase. The trend remains similar to the cases of localization length and IPR. To extract scaling function, we consider the following ansatz,

$$\Delta E = L^{-z} f_3 \left( (\alpha - \alpha_c) L^{1/\nu} \right), \quad (7)$$

where  $f_3[\cdot]$  is an arbitrary function. Using the above ansatz, we obtain data collapse  $\Delta E$  and plotted in Fig. 1(c2), with their corresponding scaled axis. The obtained exponents are  $\{\nu, s, z\} = \{0.49(1), 0.49(1), 2.02(2)\}$ .

### D. Fidelity Susceptibility

A final and useful estimator that we use for characterizing the criticality is fidelity susceptibility (FS),  $\eta_Q$ , which is defined as

$$\eta_Q = \lim_{\delta\alpha \rightarrow 0} \frac{2[1 - \mathcal{F}(\alpha, \alpha + \delta\alpha)]}{(\delta\alpha)^2}, \quad (8)$$

where  $\mathcal{F}(\alpha, \alpha + \delta\alpha) = \langle \psi(\alpha) | \psi(\alpha + \delta\alpha) \rangle$  quantifies the overlapping amplitude between the ground state wave functions at

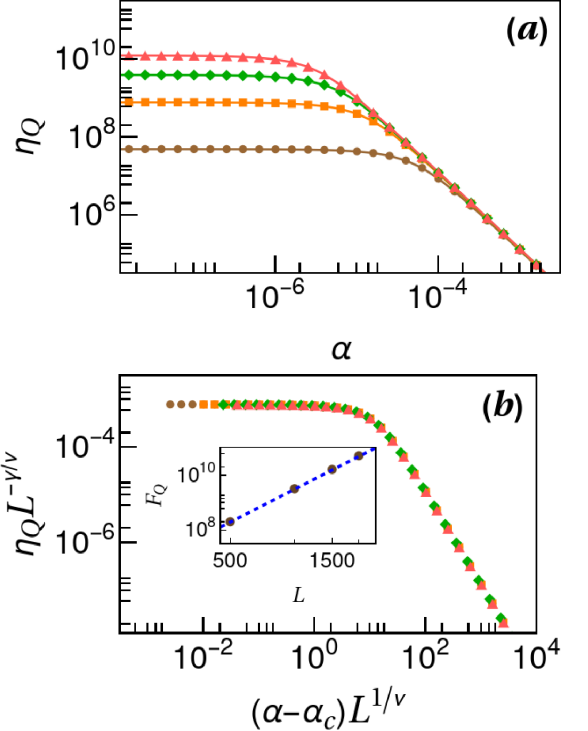


FIG. 2. (a) presents The FS,  $\eta_Q$  versus  $\alpha$  for different system sizes,  $L = 500$  (yellow circle),  $1000$  (orange square),  $15000$  (green diamond),  $2000$  (pink up-triangle) for groundstate using exact diagonalization. (b) shows a collapse plot for the  $\eta_Q$  with  $(\gamma, \nu) \approx (2.02(2), 0.49(1))$ . In the inset we plot the QFI,  $F_Q$  (brown dots), as a function of  $L$  for the ground at  $\alpha = 10^{-8}$  and we fitted it with function  $\propto L^\beta$  (blue dashed line). we found  $\beta = 3.98$ .

$\alpha$  and at  $\alpha + \delta\alpha$ , where  $\delta\alpha$  corresponds to a small shift.  $\alpha_c$  represents the boundary across which there is a drastic change in the wavefunction structure in finite systems: it is localized in the regime  $\alpha < \alpha_c$  and delocalized in the regime  $\alpha > \alpha_c$ . As a result the wavefunctions across the phases has small overlap. Within the framework, the sudden change in properties near a quantum critical point, is a feature that is effectively captured by  $\eta_Q$ .

We plot FS,  $\eta_Q$ , as a function of  $\alpha$  for various  $L$  in Fig. 2(a). As one may expect by now, the  $\eta_Q$  remains nearly flat upto the finite threshold value,  $\alpha_T$ . Finite-size effects are evident in these initial plateaus of the FS, representing the extended phase of the system. Following are the key features: First, the value of the FS dramatically enhances by increasing  $L$ . Second, the position of the maximum FS value gradually shifts towards lower  $\alpha$  with increasing  $L$ . Third, the FS becomes nearly size-independent beyond  $\alpha_T$ , indicating the system's entrance into the localized phase. The progressive drift of  $\alpha_T$  with higher  $L$  towards lower values lead it to  $\alpha_T \equiv \alpha_c \rightarrow 0^+$  in the thermodynamic limit. We propose the following ansatz for extracting the associated scaling exponents via the data collapse,

$$\eta_Q = L^{\gamma/\nu} f_6 \left( (\alpha - \alpha_c) L^{1/\nu} \right), \quad (9)$$

where  $f_6[\cdot]$  is an arbitrary function. Fig. 2(b) represents the best collapse plot that is in accordance to the cost function theory. The scaling exponents  $\gamma$  and  $\nu$  turn out to be 1.96(4) and 0.49(1), respectively.

Apart from serving as a probe of quantum criticality, fidelity susceptibility also establishes a natural bridge to the concepts in quantum parameter estimation. In particular, the fidelity susceptibility is directly proportional to the quantum Fisher information (QFI),  $\mathcal{F}_Q = 4\eta_Q$ , a quantity that characterizes the ultimate precision limits allowed by quantum mechanics when estimating an unknown parameter. Carefully designed strategies can surpass the classical precision bound, known as the standard quantum limit (SQL), and approach, or even attain, the ultimate bound set by the quantum Cramér–Rao inequality [64, 65] that sets the precision limit. Recently, critical enhancement of the QFI has been widely recognized as a resource in quantum metrology and sensing, where it enables improved parameter-estimation precision [66, 67]. The sensing performance is determined by the finite size scaling of the QFI or fidelity susceptibility with system size ( $L$ ),  $F_Q \sim L^\beta$ .  $\beta = 1$  is known as SQL, which is the best that  $L$  independent qubits can achieve [68, 69], and a quantum-enhanced sensing implies  $\beta > 1$ . Quantum criticality-based adiabatic quantum sensors that can surpass,  $\beta = 2$ , the so-called Heisenberg limit, have been previously reported in different scenarios [70–74]. Our analysis implies that  $\beta = \gamma/\nu$ , and  $\mathcal{F}_Q \sim L^4$ . Therefore, the scaling behavior extracted from the fidelity susceptibility in our model not only reveals its critical properties but also signals potential applications in criticality-assisted quantum sensing platforms.

### E. Cost Function

In order to find the best fit values of the scaling exponents we also take into account cost function,  $C_Q$ , approach, where  $C_Q$  is defined as [75, 76]

$$C_Q = \frac{\sum_{i=1}^{N-1} |Q_{i+1} - Q_i|}{\max\{Q_i\} - \min\{Q_i\}} - 1, \quad (10)$$

where  $\{Q_i\}$  is the dataset for different values of  $\alpha$  and  $L$  and  $N$  is the total number of data points in the dataset. Sorting all  $N$  values of  $|Q_i|$  according to the increasing value of  $L \text{sgn}[\alpha - \alpha_c][\alpha - \alpha_c]^\nu$ , the best scaling exponent can be found for the minimum value of cost function  $C_Q$ . Ideally, the perfect data collapse is found for  $C_Q = 0$ , i.e.,  $\sum_{i=1}^{N-1} |Q_{i+1} - Q_i| = \max\{Q_i\} - \min\{Q_i\}$ . We present certain representative cases demonstrating the behavior of the cost function around the estimated critical exponents. We plot  $C_Q$  with respect to the critical exponents  $\nu$ ,  $s$ ,  $z$  and  $\gamma$  in Figs. 3. The figures depict that the  $C_Q$  has a global minimum at  $\nu = 0.49(1)$ ,  $s = 0.49(1)$ ,  $z = 2.02(2)$  and  $\gamma = 1.96(4)$ ; data collapse is achieved with these values.

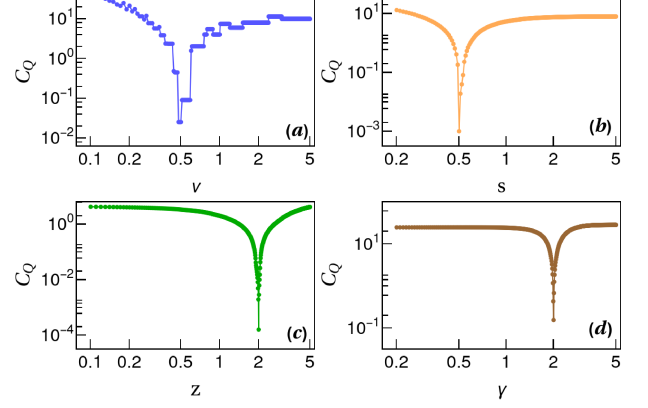


FIG. 3. Cost function to find  $\nu$ ,  $s$ ,  $z$  and  $\gamma$ . A global minimum of  $C_Q$  is at (a)  $\nu = 0.49(1)$ , (b)  $s = 0.49(1)$ , (c)  $z = 2.02(2)$ , (d)  $\gamma = 1.96(4)$ .

### IV. KIBBLE-ZUREK SCALING OF DRIVEN DYNAMICS

We now turn to the investigation of Kibble–Zurek scaling (KZS) in the driven dynamics of our model, which is intrinsically connected to the quantum criticality of phase transitions. The KZ mechanism establishes a unified framework that explains how systems produce excitations when they experience continuous phase transitions at a controlled speed. The system maintains adiabaticity when the control parameter remains distant from the criticality. The system generates unavoidable excitations because the essential energy gap approaches zero as it approaches the critical point. The KZ framework describes how adiabaticity fails during a process which starts from an easily accessible ground state before reaching a complex final state. The system is initially prepared in the localized phase and is subsequently driven across the critical point by linearly tuning the control. We linearly vary  $\alpha$  in time  $t$  with speed  $R$ . The time evolution of  $\alpha$  is given by

$$\alpha(t) = \alpha_0 + Rt, \quad (11)$$

where  $\alpha_0 < 0$  represents the initial distance from the critical point at  $t = 0$ . Within the KZS framework, adiabaticity can be maintained when the condition  $|\alpha| > R^{1/r\nu}$  is satisfied, with the scaling exponent  $r = z + 1/\nu$ . In this regime, the system can adapt to the gradual variation of the Hamiltonian and thus follow the instantaneous ground state. By contrast, when  $|\alpha| < R^{1/r\nu}$ , the intrinsic response of the system becomes slower than the external driving rate, signaling its entry into the impulse regime, where the evolution effectively freezes and excitations are generated.

To see how  $\xi$  and  $\chi$  behave around criticality while driven dynamically, we introduce following ansatz,

$$\xi = R^{-1/r} f_4 \left( \alpha R^{-1/r\nu} \right), \quad (12)$$

$$\chi = R^{-s/r\nu} f_5 \left( \alpha R^{1/r\nu} \right), \quad (13)$$

where  $f_4[\cdot]$  and  $f_5[\cdot]$  are arbitrary functions. We choose the system size  $L = 1000$ , which is large enough to ignore the

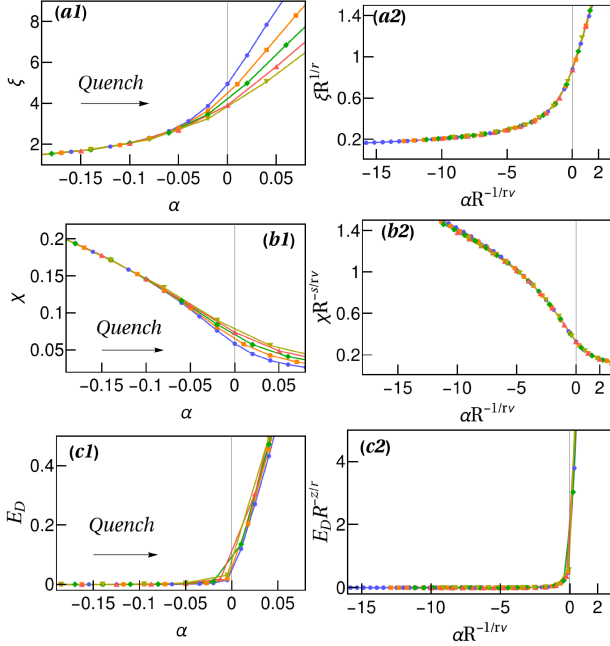


FIG. 4. Driven dynamics with the initial state being the ground state. The curves of  $\xi$  versus  $\alpha$  for  $R = 0.001$  (blue circle),  $R = 0.0015$  (orange diamond),  $R = 0.002$  (green square),  $R = 0.0025$  (pink up-triangle),  $R = 0.003$  (yellow down-triangle) (a1) before and (a2) after rescaled with  $R$ . The curves of  $\chi$  versus  $\alpha$  (b1) before and (b2) after rescaled with  $R$ . We have plotted  $E_D$  calculated from Eq. 14 versus  $\alpha$  (c1) before and (c2) after rescaled with  $R$ . The arrows in (a1), (b1) and (c1) point the quench direction. The lattice size is  $L = 1000$ .

finite-size effect in real-time simulations. We set the initial state as the ground state of the system with fixed  $\alpha_0 = -0.5$ . Fig. 4(a1) shows the evolution of the localization length  $\xi$  for different  $R$ . Initially, a strongly localized state with a small localization length  $\xi$  is almost insensitive to the ramp rate  $R$ , allowing the dynamics to closely follow the instantaneous ground state in an effectively adiabatic manner. However, as  $\alpha$  approaches to the critical point, the trajectories corresponding to different ramp rates  $R$  begin to separate, signaling the onset of the impulse regime where the evolution can no longer remain adiabatic. We rescale  $\xi$  and  $\alpha$  as  $\xi R^{1/r}$  and  $\alpha R^{-1/r\nu}$ , respectively, according to the ansatz in Eq. 12. We find that the rescaled curves collapse onto each other near the critical point, as shown in Fig. 4(a2) with the obtained scaling exponents from the static case. Similarly, Fig. 4(b1) shows the evolution of  $\chi$  for different  $R$ . In contrast to the localization length, the fidelity susceptibility starts from a large initial value and evolves through an adiabatic stage in which its behavior is nearly independent of the ramp rate  $R$ . As the system approaches the critical region, however, it exhibits a pronounced impulse response, reflecting the breakdown of adiabaticity. After rescaling  $\chi$  and  $\alpha$  as  $\chi R^{-s/\nu r}$  and  $\alpha R^{-1/\nu r}$  according to Eq. 13, respectively, we find that the rescaled curves collapse near the critical point, as shown in Fig. 4(b2).

The dynamical deviation from the instantaneous ground

state energy  $E_D$  is also an important quantity in characterizing the dynamical behavior of localization phase transitions. Its definition is given by [77]

$$E_D \equiv \text{Re} [\langle \psi(t) | H(t) | \psi(t) \rangle - E_g(t)], \quad (14)$$

where  $H(t)$  is the instantaneous Hamiltonian in the driving process, and  $E_g(t)$  is the corresponding ground state energy.  $\psi(t) = e^{-iH(t)t} \psi(0)$ , and  $\psi(0)$  is the initial state. At  $t = 0$ , away from critical point  $E_D = 0$ , and remains so; however, near criticality the energy obtained by driving  $\psi(0)$  with  $H(t)$  does not resemble the groundstate energy of the instantaneous Hamiltonian obtained through  $E_g(t)$  shown in Fig. 4(c1). This leads us to conclude that any physical state of a system, initially in equilibrium, will necessarily become excited when approaching a second-order phase transition. The driven dynamics satisfy the following ansatz:

$$E_D = R^{-z/r} f_6 \left( \alpha R^{-1/r\nu} \right), \quad (15)$$

where  $f_6[\cdot]$  is an arbitrary function. Then, by rescaling  $E_D$  and  $\alpha$  as  $R^{z/r}$  and  $\alpha R^{-1/r\nu}$ , respectively, the dynamical curves collapse onto a single universal curve, as shown in Fig. 4(c2). Thus, this dynamical scaling collapse provides independent confirmation of the critical exponents extracted from the static analysis.

## V. DISCUSSION

To summarize, in this work, we investigate localization phenomena in a one-dimensional lattice with a power-law graded hopping amplitude. This model realizes a novel kinetic route to localization, distinct from the disorder, quasiperiodic, or potential-driven mechanisms characterizing Anderson, Aubry–André, and Stark localization. In the thermodynamic limit the system becomes localized at  $|\alpha| \rightarrow 0$ , signaling the presence of a critical point characterized by a diverging localization length. Through a finite-size scaling analysis of localization length, inverse participation ratio, fidelity susceptibility, and spectral-gap, we report the associated scaling exponents revealing a new universality class. Finally, we performed complementary nonequilibrium ramp dynamics in order to further exhibit Kibble–Zurek scaling, that showed that the dynamical critical behavior can be consistently described with the static exponents. On the applied side, the sensitivity of the system near criticality suggests potential relevance for quantum metrology and sensing. Together, these results establish a coherent picture of static and dynamic scaling in our model, while also underlining the dual role of criticality as both a diagnostic tool and a practical resource.

Exploring analytic continuum descriptions and real-space field-theoretical descriptions may lead to a deeper understanding of the emergent effective potentials responsible for the observed scaling behavior. It will also be interesting to understand the effect of interaction in the realm of quantum many-body localization. Quantum simulators, such as superconducting circuits, photonic lattices, trapped ions, and ultra-

cold atoms, provide potential platforms for experimental ex-

ploration of the physics presented in this work.

---

[1] P. W. Anderson, Absence of diffusion in certain random lattices, *Phys. Rev.* **109**, 1492 (1958).

[2] S. Aubry and G. André, Analyticity breaking and anderson localization in incommensurate lattices, *Ann. Israel Phys. Soc* **3**, 18 (1980).

[3] M. Albert and P. Leboeuf, Localization by bichromatic potentials versus anderson localization, *Phys. Rev. A* **81**, 013614 (2010).

[4] A. Sahoo, U. Mishra, and D. Rakshit, Localization-driven quantum sensing, *Phys. Rev. A* **109**, L030601 (2024).

[5] G. H. Wannier, Wave functions and effective hamiltonian for bloch electrons in an electric field, *Phys. Rev.* **117**, 432 (1960).

[6] H. Fukuyama, R. A. Bari, and H. C. Fogedby, Tightly bound electrons in a uniform electric field, *Phys. Rev. B* **8**, 5579 (1973).

[7] A. R. Kolovsky and H. J. Korsch, Bloch oscillations of cold atoms in two-dimensional optical lattices, *Phys. Rev. A* **67**, 063601 (2003).

[8] A. R. Kolovsky, Interplay between anderson and stark localization in 2d lattices, *Phys. Rev. Lett.* **101**, 190602 (2008).

[9] A. R. Kolovsky and E. N. Bulgakov, Wannier-stark states and bloch oscillations in the honeycomb lattice, *Phys. Rev. A* **87**, 033602 (2013).

[10] X. He, R. Yousefjani, and A. Bayat, Stark localization as a resource for weak-field sensing with super-heisenberg precision, *Phys. Rev. Lett.* **131**, 010801 (2023).

[11] T.-C. Yi, Y.-Y. Fang, W. Chen, W.-L. You, and Y. Zhang, Unveiling quantum criticality of disordered aubry-andré-harper models via typical fidelity susceptibility, *Phys. Rev. A* **112**, 023308 (2025).

[12] C.-L. Zhai, W. Wu, C.-W. Wu, and P.-X. Chen, Stark-induced tunable phase transition in the two-photon dicke-stark model, *Phys. Rev. A* **112**, 013720 (2025).

[13] S. Banerjee, S. R. Padhi, and T. Mishra, Emergence of distinct exact mobility edges in a quasiperiodic chain, *Phys. Rev. B* **111**, L220201 (2025).

[14] A. Chakrabarty and S. Datta, Fate of wannier-stark localization and skin effect in periodically driven non-hermitian quasiperiodic lattices, *Phys. Rev. B* **111**, 174202 (2025).

[15] J.-L. Dong, E.-W. Liang, S.-Y. Liu, G.-Q. Zhang, L.-Z. Tang, and D.-W. Zhang, Critical properties in the non-hermitian aubry-andré-stark model, *Phys. Rev. B* **111**, 174209 (2025).

[16] L.-N. Wu and A. Eckardt, Bath-induced decay of stark many-body localization, *Phys. Rev. Lett.* **123**, 030602 (2019).

[17] M. Schulz, C. A. Hooley, R. Moessner, and F. Pollmann, Stark many-body localization, *Phys. Rev. Lett.* **122**, 040606 (2019).

[18] E. van Nieuwenburg, Y. Baum, and G. Refael, From bloch oscillations to many-body localization in clean interacting systems, *Proceedings of the National Academy of Sciences* **116**, 9269 (2019).

[19] D. S. Bhakuni, R. Nehra, and A. Sharma, Drive-induced many-body localization and coherent destruction of stark many-body localization, *Phys. Rev. B* **102**, 024201 (2020).

[20] S. R. Taylor, M. Schulz, F. Pollmann, and R. Moessner, Experimental probes of stark many-body localization, *Phys. Rev. B* **102**, 054206 (2020).

[21] X. Wei, X. Gao, and W. Zhu, Static and dynamical stark many-body localization transition in a linear potential, *Phys. Rev. B* **106**, 134207 (2022).

[22] J. Billy, V. Josse, Z. Zuo, A. Bernard, B. Hambrecht, P. Lugan, D. Clément, L. Sanchez-Palencia, P. Bouyer, and A. Aspect, Direct observation of anderson localization of matter waves in a controlled disorder, *Nature* **453**, 891–894 (2008).

[23] G. Roati, C. D'Errico, L. Fallani, M. Fattori, C. Fort, M. Zaccanti, G. Modugno, M. Modugno, and M. Inguscio, Anderson localization of a non-interacting bose-einstein condensate, *Nature* **453**, 895 (2008).

[24] B. Deissler, M. Zaccanti, G. Roati, C. D'Errico, M. Fattori, M. Modugno, G. Modugno, and M. Inguscio, Delocalization of a disordered bosonic system by repulsive interactions, *Nature physics* **6**, 354 (2010).

[25] M. Schreiber, S. S. Hodgman, P. Bordia, H. P. Lüschen, M. H. Fischer, R. Vosk, E. Altman, U. Schneider, and I. Bloch, Observation of many-body localization of interacting fermions in a quasirandom optical lattice, *Science* **349**, 842 (2015).

[26] W. Morong, F. Liu, P. Becker, K. Collins, L. Feng, A. Kyprianidis, G. Pagano, T. You, A. Gorshkov, and C. Monroe, Observation of stark many-body localization without disorder, *Nature* **599**, 393 (2021).

[27] Y. Guo, S. Dhar, A. Yang, Z. Chen, H. Yao, M. Horvath, L. Ying, M. Landini, and H.-C. Nägerl, Observation of many-body dynamical localization, *Science* **389**, 716 (2025).

[28] R. P. A. Lima, H. R. da Cruz, J. C. Cressoni, and M. L. Lyra, Finite-size scaling of power-law bond-disordered anderson models, *Phys. Rev. B* **69**, 165117 (2004).

[29] H. Cheraghchi, S. M. Fazeli, and K. Esfarjani, Localization-delocalization transition in a one one-dimensional system with long-range correlated off-diagonal disorder, *Phys. Rev. B* **72**, 174207 (2005).

[30] F. de Moura, Absence of localization on the 2d model with long-range correlated off-diagonal disorder, *The European Physical Journal B* **78**, 335 (2010).

[31] W. Dias, F. de Moura, M. Coutinho-Filho, and M. Lyra, Kosterlitz-thouless-like transition in two-dimensional lattices with long-range correlated hopping terms, *Physics Letters A* **374**, 3572 (2010).

[32] T. Assunção, M. Lyra, F. de Moura, and F. Domínguez-Adame, Coherent electronic dynamics and absorption spectra in an one-dimensional model with long-range correlated off-diagonal disorder, *Physics Letters A* **375**, 1048 (2011).

[33] C.-S. Deng and H. Xu, Delocalization to localization transition in one-dimensional systems with long-range correlated off-diagonal disorder, *Physica E: Low-dimensional Systems and Nanostructures* **44**, 1473 (2012).

[34] A. Saha and D. Rakshit, Localization with non-hermitian off-diagonal disorder, *arXiv preprint arXiv:2310.13744* (2023).

[35] H. Tabanelli, C. Castelnovo, and A. Štrkalj, Reentrant localization transitions and anomalous spectral properties in off-diagonal quasiperiodic systems, *Phys. Rev. B* **110**, 184208 (2024).

[36] J. Dziarmaga, Dynamics of a quantum phase transition and relaxation to a steady state, *Advances in Physics* **59**, 1063 (2010).

[37] A. Polkovnikov, K. Sengupta, A. Silva, and M. Vengalattore, Colloquium: Nonequilibrium dynamics of closed interacting quantum systems, *Rev. Mod. Phys.* **83**, 863 (2011).

[38] T. Kibble, Phase-transition dynamics in the lab and the uni-

verse, *Physics Today* **60**, 47 (2007).

[39] T. W. B. Kibble, Topology of cosmic domains and strings, *Journal of Physics A: Mathematical and General* **9**, 1387 (1976).

[40] W. H. Zurek, Cosmological experiments in superfluid helium?, *Nature* **317**, 505 (1985).

[41] W. Zurek, Cosmological experiments in condensed matter systems, *Physics Reports* **276**, 177 (1996).

[42] W. H. Zurek, U. Dorner, and P. Zoller, Dynamics of a quantum phase transition, *Phys. Rev. Lett.* **95**, 105701 (2005).

[43] J. Dziarmaga, Dynamics of a quantum phase transition: Exact solution of the quantum ising model, *Phys. Rev. Lett.* **95**, 245701 (2005).

[44] A. Polkovnikov, Universal adiabatic dynamics in the vicinity of a quantum critical point, *Phys. Rev. B* **72**, 161201 (2005).

[45] B. Damski and W. H. Zurek, Dynamics of a quantum phase transition in a ferromagnetic bose-einstein condensate, *Phys. Rev. Lett.* **99**, 130402 (2007).

[46] D. Sen, K. Sengupta, and S. Mondal, Defect production in non-linear quench across a quantum critical point, *Phys. Rev. Lett.* **101**, 016806 (2008).

[47] A. Bermudez, D. Patanè, L. Amico, and M. A. Martin-Delgado, Topology-induced anomalous defect production by crossing a quantum critical point, *Phys. Rev. Lett.* **102**, 135702 (2009).

[48] S. Deng, G. Ortiz, and L. Viola, Dynamical non-ergodic scaling in continuous finite-order quantum phase transitions, *Europhysics Letters* **84**, 67008 (2009).

[49] A. Chandran, F. J. Burnell, V. Khemani, and S. L. Sondhi, Kibble-zurek scaling and string-net coarsening in topologically ordered systems, *Journal of Physics: Condensed Matter* **25**, 404214 (2013).

[50] Y. Huang, S. Yin, B. Feng, and F. Zhong, Kibble-zurek mechanism and finite-time scaling, *Phys. Rev. B* **90**, 134108 (2014).

[51] G. m. H. Roósz, U. Divakaran, H. Rieger, and F. Igliói, Nonequilibrium quantum relaxation across a localization-delocalization transition, *Phys. Rev. B* **90**, 184202 (2014).

[52] L. Morales-Molina, E. Doerner, C. Danieli, and S. Flach, Resonant extended states in driven quasiperiodic lattices: Aubry-andré localization by design, *Phys. Rev. A* **90**, 043630 (2014).

[53] M. Serbyn, Z. Papić, and D. A. Abanin, Quantum quenches in the many-body localized phase, *Phys. Rev. B* **90**, 174302 (2014).

[54] C.-W. Liu, A. Polkovnikov, A. W. Sandvik, and A. P. Young, Universal dynamic scaling in three-dimensional ising spin glasses, *Phys. Rev. E* **92**, 022128 (2015).

[55] A. Sinha, M. M. Rams, and J. Dziarmaga, Kibble-zurek mechanism with a single particle: Dynamics of the localization-delocalization transition in the aubry-andré model, *Phys. Rev. B* **99**, 094203 (2019).

[56] X. Bu, L.-J. Zhai, and S. Yin, Quantum criticality in the disordered aubry-andré model, *Phys. Rev. B* **106**, 214208 (2022).

[57] X. Bu, L.-J. Zhai, and S. Yin, Kibble-zurek scaling in one-dimensional localization transitions, *Phys. Rev. A* **108**, 023312 (2023).

[58] E.-W. Liang, L.-Z. Tang, and D.-W. Zhang, Quantum criticality and kibble-zurek scaling in the aubry-andré-stark model, *Phys. Rev. B* **110**, 024207 (2024).

[59] X.-Y. Wang, W.-J. Yu, Y.-M. Sun, and L.-J. Zhai, Driven dynamics of localization phase transition in the aubry-andré model with initial gapless extended states, *arXiv preprint arXiv:2509.06358* (2025).

[60] C. Meldgin, U. Ray, P. Russ, D. Chen, D. M. Ceperley, and B. DeMarco, Probing the bose glass-superfluid transition using quantum quenches of disorder, *Nature Physics* **12**, 646 (2016).

[61] M. Anquez, B. A. Robbins, H. M. Bharath, M. Boguslawski, T. M. Hoang, and M. S. Chapman, Quantum kibble-zurek mechanism in a spin-1 bose-einstein condensate, *Phys. Rev. Lett.* **116**, 155301 (2016).

[62] L. W. Clark, L. Feng, and C. Chin, Universal space-time scaling symmetry in the dynamics of bosons across a quantum phase transition, *Science* **354**, 606 (2016).

[63] C. S. Chiu, G. Ji, A. Masurenko, D. Greif, and M. Greiner, Quantum state engineering of a hubbard system with ultracold fermions, *Phys. Rev. Lett.* **120**, 243201 (2018).

[64] H. Cramér, *Mathematical methods of statistics*, Vol. 26 (Princeton university press, 1999).

[65] S. L. Braunstein and C. M. Caves, Statistical distance and the geometry of quantum states, *Phys. Rev. Lett.* **72**, 3439 (1994).

[66] V. Montenegro, C. Mukhopadhyay, R. Yousefjani, S. Sarkar, U. Mishra, M. G. Paris, and A. Bayat, Review: Quantum metrology and sensing with many-body systems, *Physics Reports* **1134**, 1 (2025).

[67] K. D. Agarwal, S. Mondal, A. Sahoo, D. Rakshit, A. S. De, and U. Sen, Quantum sensing with ultracold simulators in lattice and ensemble systems: a review, *arXiv preprint arXiv:2507.06348* (2025).

[68] V. Giovannetti, S. Lloyd, and L. Maccone, Quantum-enhanced measurements: Beating the standard quantum limit, *Science* **306**, 1330 (2004).

[69] V. Giovannetti, S. Lloyd, and L. Maccone, Quantum metrology, *Phys. Rev. Lett.* **96**, 010401 (2006).

[70] S. Mondal, A. Sahoo, U. Sen, and D. Rakshit, Multicritical quantum sensors driven by symmetry-breaking, *arXiv:2407.14428* (2024).

[71] A. Sahoo and D. Rakshit, Enhanced sensing of stark weak field under the influence of aubry-andré \{\'e}-harper criticality, *arXiv:2408.03232* (2024).

[72] A. Sahoo, A. Saha, and D. Rakshit, Stark localization near aubry-andré criticality, *Phys. Rev. B* **111**, 024205 (2025).

[73] A. Debnath, M. Gajda, and D. Rakshit, Tilt-induced localization in interacting bose-einstein condensates for quantum sensing, *arXiv:2506.06173* (2025).

[74] A. Sahoo and D. Rakshit, Power-law interactions stabilize time crystals realizing quantum energy storage and sensing, *arXiv:2508.14847* (2025).

[75] J. Šuntajs, J. Bonča, T. c. v. Prosen, and L. Vidmar, Ergodicity breaking transition in finite disordered spin chains, *Phys. Rev. B* **102**, 064207 (2020).

[76] R. Modak, D. Rakshit, and U. Sen, Finite-size scalings in measurement-induced dynamical phase transition, *arXiv preprint arXiv:2107.14647* (2021).

[77] L.-J. Zhai, G.-Y. Huang, and S. Yin, Nonequilibrium dynamics of the localization-delocalization transition in the non-hermitian aubry-andré model, *Phys. Rev. B* **106**, 014204 (2022).